






Analysis of Ensemble of Neural Networks and Fuzzy Logic Classification in Process of Semantic Segmentation of Martian Geomorphological Settings

Kamil Choromański¹^a, Joanna Kozakiewicz²^b, Mateusz Sobucki³^c,
Magdalena Pilarska-Mazurek¹^d and Robert Olszewski¹^e

¹Faculty of Geodesy and Cartography, Warsaw University of Technology, Plac Politechniki 1, 00-665 Warsaw, Poland

²Faculty of Physics, Astronomy and Applied Computer Science, Jagiellonian University, prof. Stanisława Łojasiewicza 11, 30-348 Krakow, Poland

³Faculty of Geography and Geology, Jagiellonian University, Gronostajowa 7, 30-387 Krakow, Poland

Keywords: Deep Learning, Semantic Segmentation, Mars, CNNs, FIS, Aeolian Landscape.

Abstract: Deep learning analysis of multisource Martian data (both from orbiter and rover) allows for the separation and classification of different geomorphological settings. However, it is difficult to determine the optimal neural network model for unambiguous semantic segmentation due to the specificity of Martian data and blurring of the boundary of individual settings (which is its immanent property). In this paper, the authors describe several variants of multisource deep learning processing system for Martian data and develop a methodology for semantic segmentation of geomorphological settings for this planet based on the combination of selected solutions output. Network ensemble with use of the weighted averaging method improved results comparing to single network. The paper also discusses the decision rule extraction method of individual Martian geomorphological landforms using fuzzy inference systems. The results obtained using FIS tools allow for the extraction of single geomorphological forms, such as ripples.

1 INTRODUCTION


Mapping of landforms on Mars using remote sensing data has become one of the most important issues in space exploration in recent years. The further development in Mars exploration requires preparation of detailed geomorphological maps. The amount of high-resolution data acquired by Martian orbiters and rovers increases very quickly, covering vast regions of the planetary surface. Mapping of these areas in a short period of time can be done only using automatic methods. In this work, we present a novel approach to map aeolian landscape on Mars using deep learning analysis. We focused on combining multiple models trained on multisource


data (namely orbital imagery, derivatives of elevation models and in situ data from rover camera), taking advantage of ensemble methods. We also analysed use of fuzzy inference systems in the process of decision rule extraction and individual landforms' classification.


2 RELATED WORKS


2.1 Martian Geomorphological Landforms


Mars is a desert planet covered by many aeolian (wind related) landforms, such as dunes or ripples. In

^a <https://orcid.org/0000-0002-2047-7434>

^b <https://orcid.org/0000-0002-9264-8298>

^c <https://orcid.org/0000-0002-2958-8966>

^d <https://orcid.org/0000-0001-9494-9863>

^e <https://orcid.org/0000-0003-1697-9367>

this work, we will focus on ripples as they are the most common features in the Martian landscape. Ripples are sand ridges ranging from centimetres to meters and formed by wind perpendicular to their crests. Automatic detection of areas covered by large (> 20 cm in height) ripples are particularly important for Martian investigation, as ripples often become traps for wheeled vehicles (e.g., Squyres et al. 2006). We will focus on the area of Meridiani Planum (Hynek et al., 2002), which is one of the best-known regions on Mars due to extensive in situ and orbital investigations. This is a flat region covered by impact craters and ripples (see e.g. Fenton et al., 2015). In this area there are three distinct geomorphological settings: (i) ripple fields – ripples on sand covers, (ii) ripples on bedrock - areas where extensive erosion led to exposing the bedrock in spaces between ripples, and (iii) sand-gravel covers – extensive sand-gravel sheets. Two other (not aeolian) landforms characteristic of this region are impact craters and structural lineaments.

2.2 Automated Segmentation of Geomorphological Landforms

First approaches to automated segmentation of Martian geomorphological landforms were proposed in the beginning of 21st century (Stepinski et al., 2006; Stepinski et al., 2009; Gosh et al., 2010). Well-known machine learning algorithms were utilized for this task (Stepinski et al., 2006). As Martian data volumes and computing power increased, Deep learning (DL) algorithms have begun to be used. Semantic segmentation based on DL approach was utilized both for impact craters (Lee, 2019; Bandeira, 2012; Stepinski et al., 2006; Stepinski et al., 2009) and landforms (Palafox et al., 2017; Barrett et al., 2022; Nagle-Mcnaughton et al., 2020). DL techniques have been employed successfully on the most widely used imagery and elevation data sources collected from Mars: Mars Orbiter Laser Altimeter (MOLA) (Stepinski et al., 2006), High Resolution Stereo Camera (HRSC) (Lee, 2019), Context Camera (CTX) (Palafox et al., 2017) and High Resolution Imaging Science Experiment (HiRISE) (Wilhelm et al., 2020).

There are also works taking advantage of images taken by Martian rovers for the purposes of segmentation and detection of terrain forms (Wagstaff et al., 2018).

So far, a study by (Rothrock et al., 2016) is the only one using orbital and rover data in one workflow. However, these two data sources were used in separation and for different purposes (orbital data was used for search of optimal landing site for

future rovers and rover data for wheel slip predictions). In this work, we propose an approach that utilizes multiple data sources for semantic segmentation of geomorphological settings basing on deep learning multi-source data fusion methods proposed by (Cao et al., 2018).

2.3 Decision Fusion

There are numerous works proving that fusing decision outputs from various neural network models may improve accuracy and generalizability comparing to use of a single model. Ensemble of neural networks was used with success both for recurrent (Zhou et al., 2018) and convolutional neural networks (Manna et al., 2021; Han and Jeong, 2020). Simple methods such as averaging, weighted averaging or majority voting are being used in many works. Some researchers are developing also more sophisticated approaches (Manna et al., 2021).

3 EXPERIMENTAL DESIGN

3.1 Data Sources and Pre-processing

In our investigation we used orbital and in situ data, simultaneously. We used the high-resolution orbital images of the Martian surface obtained by HiRISE onboard the NASA Mars Reconnaissance Orbiter mission. The orbital data were supplemented by in situ data obtained by the Opportunity rover, one of two rovers of the NASA Mars Exploration Rover (MER) mission. Opportunity explored the western part of Meridiani Planum between Eagle and Endeavour craters in years 2004-2018.

The HiRISE and Opportunity Rover data were downloaded from the Planetary Data System (PDS). To study aeolian landforms from the planetary surface we focused on the Navigation Camera (NAVCAM) data. The NAVCAM system consisted of two stereoscopic cameras (Maki et al., 2003).

3.1.1 HiRISE Data

We used eight images to produce four stereo pairs and to create the Digital Terrain Model (DTM) that covered the entire Opportunity rover traverse: ESP_018846_1775-ESP_018701_1775,

ESP_051245_1780-ESP_020758_1780,
ESP_016644_1780-ESP_037109_1780,
PSP_001414_1780-PSP_005423_1780.

The HiRISE data were processed using NASA Ames Stereo Pipeline (ASP) (version v2.6.2) and Integrated Software for Imagers and Spectrometers (ISIS) (version 3.6.0). From the HiRISE stereopairs four DTMs were produced. Selected HiRISE images were orthorectified using the DTMs to remove the impact of terrain height on the geometry of the images. Finally, the orthoimages and the DTMs were mosaicked into continuous raster file, so-called mosaic, which covered an area of approximately 87 square km and had a spatial resolution of 27 cm.

Using elevation-DTM data from HiRISE images, the authors also developed derived relief models: topographic roughness index (TRI), topographic positioning index (TPI). Various curvature models, e.g., transverse, longitudinal, were also determined from the DTM analysis.

3.1.2 NAVCAM Data

We stitched NAVCAM images into spatially referenced panoramas basing on NAVCAM images metadata. Radiometric differences between panorama segments were reduced using histogram matching technique. The final panoramas were cylinder-projected. Areas, where images were overlapping were merged by selecting every second pixel of each image. The starting orientation for each panorama is north to ensure consistency for the analysis of all panoramas used in the research process. The resolution of a single output panorama is 2048×6992.

Finally, semantic features from each panorama were extracted with the use of Places-CNN network pre-trained on Places365 dataset (Zhou et al., 2017). Each panorama was converted to 2048-dimensional feature vector which was reduced to 50 dimensions by using principal component analysis (PCA) method. To spatially align in-situ data with orbital data we interpolated feature vectors onto spatial domain using Nadaraya-Watson interpolation algorithm.

3.2 Semantic Segmentation Network

We use a single architecture of a convolutional neural network (CNN) to train a few independent models in order to create semantic segmentation of terrain. Different data sources were used as the input for these models.

A CNN encoder-decoder network consisting of two encoders and one decoder was used to train models employed in this research. Both encoders of the network were based on VGG-16 architecture

(Simonyan and Zisserman, 2015) with last (fifth) layer of original VGG-16 replaced by two convolutional layers. First encoder was used to extract semantic features from orbital data (imagery data and derivatives of elevation model concatenated into multi-layer raster are fed into this part of model). Second one was utilized to extract in-situ features. Every last layer of each block of the second encoder was concatenated with corresponding layer of the first encoder. The decoder block was also based on VGG-16 (without the last block, with an up-sampling layer instead of max-pooling and with reduced number of parameters). Semantic segmentation of orbital image is generated as an output from decoder block. The architecture was implemented using a TensorFlow framework (Martin, 2015).

3.3 Averaging

Two averaging methods were utilized in this research: i) simple averaging of selected models decision certainty, ii) weighted averaging.

In the first case, class decision certainty values of each model for each data point (pixel) x_i were summed and divided by number of models (n):

$$\bar{x} = \frac{\sum_{i=1}^n x_i}{n} \quad (1)$$

Weighted averaging \bar{x}_w was performed by assigning weight w_i to each of n models based on their performance on test dataset (assessed by overall accuracy). The final decision certainty was computed as the weighted average for each data point x_i :

$$\bar{x}_w = \frac{\sum_{i=1}^n w_i * x_i}{\sum_{i=1}^n w_i} \quad (2)$$

Finally, class with the highest fused decision certainty value was selected as valid for a given data point.

3.4 Fuzzy Logic

Using deep machine learning methods allows to obtain reliable classification results, however, the limitation of this approach is the so-called black box associated with the use of neural networks. In order to obtain explicitly defined (yet intentionally fuzzy) decision rules for classification, the authors of this paper have applied fuzzy inference systems (FIS). This approach allows the extraction of decision rules, but requires prior training of the neural network and obtaining reliable parameters of membership of pixels to geomorphological setting classes.

4 EXPERIMENTS AND ANALYSIS

4.1 Individual Models Training

The network architecture described above was used to train a few semantic segmentation models using different input data combinations (Table 1).

Table 1: Summary of data sources used for each experiment.

Experiment no.	Data used
1	orbital only
2	orbital + TPI/TRI
3	orbital + curvatures
4	Orbital and in situ fused
5	Orbital and in situ fused + TPI/TRI
6	Orbital and in situ fused + curvatures

Each network was trained on the same amount of data, namely: 523 256x256 tiles of each data type for training and 108 tiles for testing. As the training dataset was not large, offline data augmentation techniques were utilized in order to enlarge dataset. Moreover, both VGG-16 encoders were pretrained on the ImageNet dataset.

In our analysis, we used a system of four classes of Meridiani Planum geomorphological setting:

- 1) ripple fields,
- 2) ripples on bedrock,
- 3) sand-gravel covers,
- 4) others, neglected in results analysis

4.2 Averaging

Two approaches of results averaging were tested: i) simple averaging with use of chosen models, and ii) weighted averaging.

Taking into account individual models results a couple of variations of models were selected for simple averaging. Table 2 summarizes experiments conducted to check the effectiveness of simple averaging technique.

Second approach to averaging is to use weights assigned to each model. We used ranked-based approach to weighting where constant weight values were assigned to models basing on their individual accuracy scores (see point 5.1). Table 3 shows weights assigned to each model.

Table 2: Summary of experiments carried out with use of simple averaging technique.

Experiments no. used for averaging (see Table 1)
1,2,5,6
5,6
2,5
2,3,4,5
4,5
4,5,6
1,2,3,4,5,6

Table 3: Weight value assigned to each experiment basing on its individual results.

Experiment no. (see Table 1)	Weight value
1	0.05
2	0.20
3	0.10
4	0.15
5	0.50
6	0.00

As one can observe, experiment no. 6 was excluded from multi-model decision process due to its significantly worse individual performance.

4.3 Fuzzy Logic based Approach

The use of FIS systems allows for the extraction of fuzzy decision rules and the development of an efficient inference system based on multiple variables. In this work, Takagi-Sugeno-Kang fuzzy inference FIS models (Sugeno, 1985) were used. This approach uses singleton output membership functions that are either constant or a linear function of the input values. Three FIS models were developed to classify Martian aeolian settings. A fuzzy tree - Aggregated Structure was also constructed. In this approach, input values are incorporated as groups at the lowest level, where each input group is fed into a FIS (Siddique, 2013). The outputs of the lower level fuzzy systems are aggregated using the higher level fuzzy systems. In this work, for the simplicity of the model, only two explanatory variables: image value (IMG) and TRI, and several simple linguistic variables: low, medium, high, possible etc. were used.

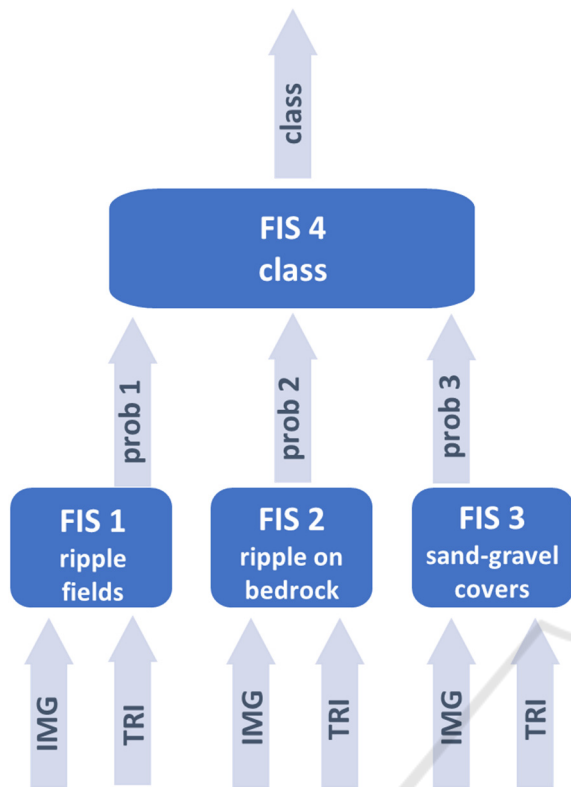


Figure 1: Aggregated Fuzzy Tree.

4.4 Evaluation Metrics

To assess results of the conducted experiments both global and per-class evaluation metrics were used, namely: overall pixel accuracy, per-class precision, recall and F1 score. Also, averaged values of per-class precision, per-class recall, and per-class F1 score were used to assess overall performance of selected approaches.

Overall pixel accuracy:

$$acc = \frac{tr(CM)}{N} \quad (3)$$

Where tr is the trace of the matrix, CM is the confusion matrix, and N is the number of pixels in all classes.

Per-class precision, P_c :

$$P_c = \frac{CM_{cc}}{\sum_{j=1}^n CM_{cj}} \quad (4)$$

Per-class recall, r_c :

$$r_c = \frac{CM_{cc}}{\sum_{j=1}^n CM_{jc}} \quad (5)$$

Where c represents the index of a given class in the confusion matrix, n is the number of all classes, and CM_{ij} is the i th row and the j th column element in the confusion matrix.

The per-class F1 score takes precision and recall metrics into account:

$$F1 = \frac{2 * P_c * r_c}{P_c + r_c} \quad (6)$$

5 RESULTS

Predictions on test dataset of individual and ensembled models were compared with use of evaluation metrics described in chapter 4.4.

5.1 Individual Models

Models trained using different data sources combinations (Table 1) varied between 91.88% and 95.94% in terms of overall accuracy on test dataset. Best results regarding majority of metrics were achieved in the experiment which used both in situ and orbital data along with TPI and TRI rasters (experiment no. 5).

Figure 2 shows results achieved by the best model with comparison to the per-metric best and the per-metric worst result. It can be observed that not in every case best individual model gives the best result for each of the tested classes.

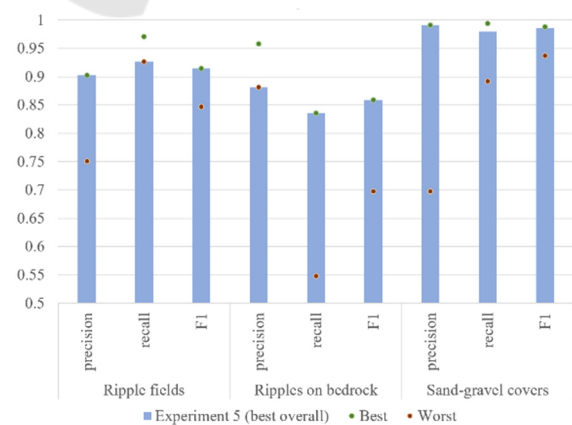


Figure 2: Precision, recall and F1-score comparison of best individual model and best and worst results from all models for each class.

5.2 Ensemble Techniques

The results of simple averaging experiments using different models (Table 2) are visualized below (Figure 3). Mean value of precision, recall and F1 score was computed basing on results for individual classes. Best overall simple averaging results were achieved using combination of two models: 4 and 5. However, the results were better only in terms of precision metric when compared to best individual model (no. 5). Also, overall accuracy of simple averaging methods is lower than achieved by model no. 5. (see Figure 5).

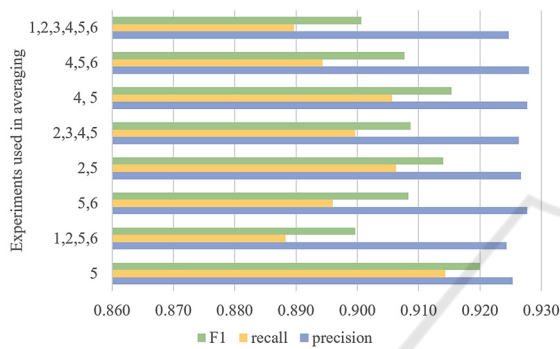


Figure 3: Mean precision, recall and F1-score comparison of best individual model (5) and multiple models combined with use of simple averaging technique.

Weighted averaging technique was tested using weights introduced in Table 3 and compared to selected results from simple averaging and best individual model. Figure 4 shows comparison of achieved precision, recall and F1-score. Figure 5 compares overall accuracy of each model.

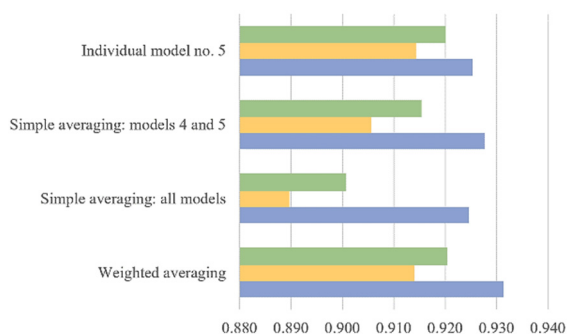


Figure 4: Mean precision, recall and F1-score comparison of best individual model (5), selected multiple models combined with use of simple averaging technique and models combined with use of weighted averaging technique.

Weighted approach proved to give better or equal results when compared to any individual model in terms of precision, recall and F1-score. Overall accuracy is also better than any other approach tested in this research and achieved level of 96.10%.

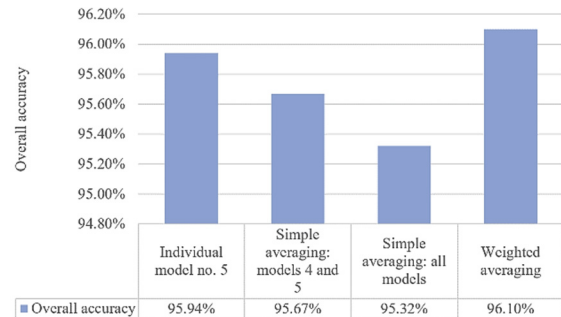


Figure 5: Overall accuracy of best individual model (5), selected multiple models combined with use of simple averaging technique and model combined with use of weighted averaging technique.

The weighted averaging technique produces results that visually fit well with manual recognition of the geomorphological settings. It enables distinction of the ripples on bedrock class in areas with small share of bedrock surface. Subsequently, it tends to overlook small, isolated bedrock outcrops, which prevents creation of small, misleading artifacts (Figure 6). The weighted averaging results tend to have lower, however still conclusive, decision certainty value in ambiguous areas than some other approaches. It opens a prospect for better multi-aspect terrain recognition using fuzzy logic.

5.3 Fuzzy Logic Classification

In the present study, an aggregate decision tree was developed to detect individual Martian geomorphological landforms. Each of the three source Sugeno trees allows for classification of a distinct type of landform (e.g. ripples) and extraction of decision rules. For example, first FIS (Figure 1) component of the FIS tree allows classification of ripples based on two decision variables - IMG and the morphometric parameter TRI. The nonlinear FIS decision surface is shown in Figure 7. The operation of this FIS tree is based on only three fuzzy decision rules:

- if IMG is *medium* and TRI is *medium* then ripple is *certain*
- if IMG is *low* and TRI is *low* then ripple is *possible*
- if IMG is *high* or TRI is *high* then ripple is *impossible*

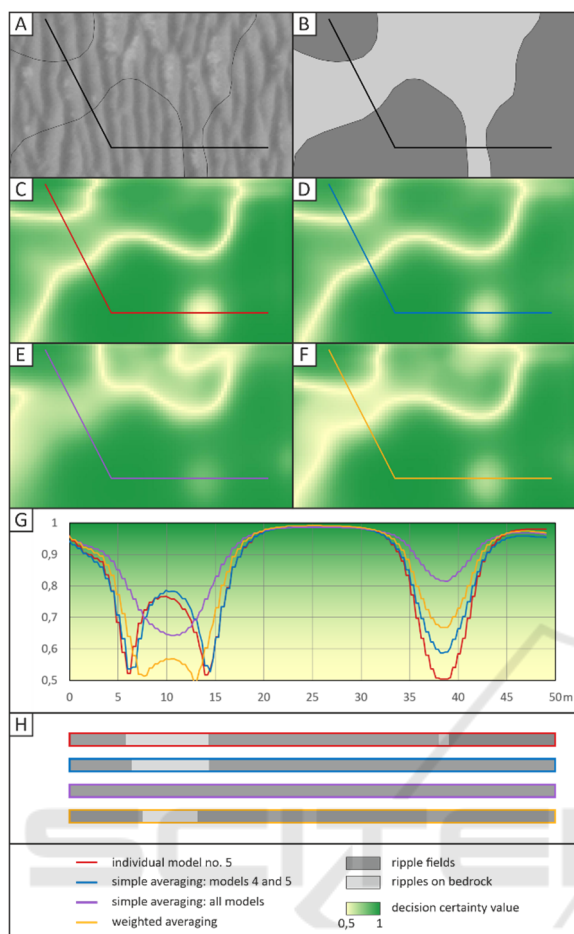


Figure 6: Exemplary part of classified terrain; orthoimage (A), manual labelling (B), individual model no.5 (C), simple averaging: model 4 and 5 (D), simple averaging: all models (E), weighted averaging (F), decision certainty value plot for a chosen profile (G), classification result along the profile for different approaches (H).

The results obtained are (in terms of accuracy) much worse than the classification based on neural networks (71.23% classification correctness), but this is partly due to the way the results are granulated (Figure 8). The FIS system classifies as "ripple" not so much the areas of ripple occurrence, but individual ripples. The areas in between ripples have been assigned to a different feature class: non-ripples. Thus, the obtained results allow both to "reveal" the decision rules and open new research directions in the field of neuro-fuzzy classification.

6 CONCLUSIONS

This research has shown that use of deep learning methods combined with multisource data have big

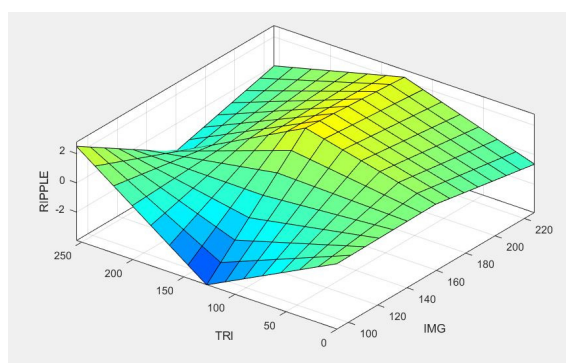


Figure 7: Nonlinear fuzzy decision surface.

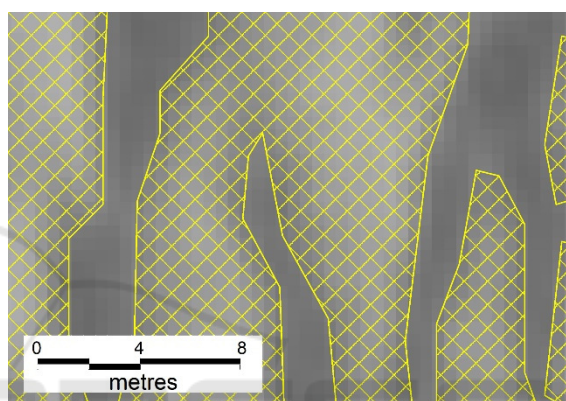


Figure 8: FIS classification of ripples using decision variables: image value and TRI.

potential for the highly accurate, automated geomorphological Martian settings segmentation. These results may be improved further with use of ensemble methods such as weighted averaging.

Fusion of multiple model decisions with varying accuracy may bring improvement in comparison to use of one model. Weighted averaging proved to give better results than simple averaging with regard to model decision fusion for semantic segmentation of geomorphological settings. Automated optimization of weight values may further increase system accuracy and such approach will be investigated in future.

The use of deep learning machine learning methods allows for the correct classification of aeolian forms on Mars and, consequently, for the development of an implicit knowledge base acting on the "black box" principle. The use of fuzzy logic allows the extraction of decision rules which explain why a given pixel has been classified into the specific geomorphological setting class. The decision fuzzy rules provide an understanding of the multifactorial reasons for classifying pixels into a given category and the development of an explicit knowledge base.

Subsequently, the FIS system enables individual forms (e.g. ripples) recognition. These issues will be further investigated by the authors of this paper.

ACKNOWLEDGEMENTS

Funding: The work was funded by the Anthropocene Priority Research Area budget under the program "Excellence Initiative – Research University" at the Jagiellonian University and by POB Research Centre Cybersecurity and Data Science of Warsaw University of Technology within the Excellence Initiative Program - Research University (ID-UB).

REFERENCES

- Moore, R., Lopes, J. (1999). Paper templates. In *TEMPLATE'06, 1st International Conference on Template Production*. SCITEPRESS.
- Smith, J. (1998). *The book*, The publishing company. London, 2nd edition.
- Manna, A., Kundu, R., Kaplun, D. et al. (2021). *A fuzzy rank-based ensemble of CNN models for classification of cervical cytology*. *Sci Rep* 11, 14538
- Zhou, J., Tian P., Chu Z., and Na S. (2018). *Data Pre-Analysis and Ensemble of Various Artificial Neural Networks for Monthly Streamflow Forecasting*. *Water* 10, no. 5: 628.
- Han S., Jeong J., (2020). *An Weighted CNN Ensemble Model with Small Amount of Data for Bearing Fault Diagnosis*. *Procedia Computer Science*, V. 175
- K. Simonyan, A. Zisserman, (2015). *Very deep convolutional networks for large-scale image recognition*. 3rd International Conference on Learning Representations, ICLR 2015—Conference Track Proceedings, pp. 1–14.
- T. F. Stepinski, S. Ghosh, R. Vilalta, (2006). *Automatic Recognition of Landforms on Mars Using Terrain Segmentation and Classification*. In *Proceedings of the 9th International Conference on Discovery Science*, LNAI 4265, pp. 255–266.
- T. F. Stepinski, M. P. Mendenhall, B. D. Bue, (2009). *Machine cataloging of impact craters on Mars*. *Icarus*, 203(1), pp. 77–87. <https://doi.org/10.1016/j.icarus.2009.04.026>
- S. Ghosh, T. F. Stepinski, R. Vilalta, (2010). *Automatic annotation of planetary surfaces with geomorphic labels*. *IEEE Transactions on Geoscience and Remote Sensing*, 48(1), pp. 175–185. <https://doi.org/10.1109/TGRS.2009.2027113>
- C. Lee, (2019). *Automated crater detection on Mars using deep learning*. *Planetary and Space Science*, 170(2015), pp. 16–28. <https://doi.org/10.1016/j.pss.2019.03.008>
- L. Bandeira, W. Ding, T. Stepinski, (2012). *Detection of sub-kilometer craters in high resolution planetary images using shape and texture features*. *Advances in Space Research*, 49(1), pp. 64–74. <https://doi.org/10.1016/j.asr.2011.08.021>
- L. F. Palafox, C. W. Hamilton, S. P. Scheidt, A. M. Alvarez, (2017). *Automated detection of geological landforms on Mars using Convolutional Neural Networks*. *Computers and Geosciences*, 101(January), pp. 48–56. <https://doi.org/10.1016/j.cageo.2016.12.015>
- A. M. Barrett, M. R. Balme, M. Woods, S. Karachalios, D. Petrocelli, L. Joudrier, E. Sefton-Nash, (2022). *NOAH-H, a deep-learning, terrain classification system for Mars: Results for the ExoMars Rover candidate landing sites*. *Icarus*, 371 (September 2021), 114701. <https://doi.org/10.1016/j.icarus.2021.114701>
- T. Nagle-Mcnaughton, T. McClanahan, L. Scuderi, (2020). *PlaNet: A Neural Network for Detecting Transverse Aeolian Ridges on Mars*. *Remote Sensing*, 12(21), pp. 1–15. <https://doi.org/10.3390/rs12213607>
- T. Wilhelm, M. Geis, J. Püttschneider, T. Sievernich, T. Weber, K. Wohlfarth, C. Wöhler, (2020). *DoMars16k: A Diverse Dataset for Weakly Supervised Geomorphologic Analysis on Mars*. *Remote Sensing*, 12(23), pp. 1–38. <https://doi.org/10.3390/rs12233981>
- K. L. Wagstaff, Y. Lu, A. Stanboli, K. Grimes, T. Gowda, J. Padams, (2018). *Deep Mars: CNN Classification of Mars Imagery for the PDS Imaging Atlas*. 32nd AAAI Conference on Artificial Intelligence, AAAI, pp. 7867–7872.
- B. Rothrock, J. Papon, R. Kennedy, M. Ono, M. Heverly, C. Cunningham, (2016). *SPOC: Deep Learning-based terrain classification for Mars rover missions*. *AIAA Space and Astronautics Forum and Exposition*, September 2016, pp. 1–12. <https://doi.org/10.2514/6.2016-5539>
- R. Cao, J. Zhu, W. Tu, Q. Li, J. Cao, B. Liu, Q. Zhang, G. Qiu, (2018). *Integrating Aerial and Street View Images for Urban Land Use Classification*. *Remote Sensing*, 10(10), 1553. <https://doi.org/10.3390/rs10101553>
- B. Zhou, A. Lapedriza, A. Khosla, A. Olivia, A. Torralba. (2017). *Places: A 10 Million Image Database for Scene Recognition*. 2017 IEEE Transactions on Pattern Analysis and Machine Intelligence, pp.1452-1464. <https://doi.org/10.1109/TPAMI.2017.2723009>
- A. Martin, et al. (2015). *TensorFlow: Large-scale machine learning on heterogeneous systems*. Software available from tensorflow.org
- M. Sugeno, *Industrial applications of fuzzy control*, Elsevier Science Pub. Co., 1985
- N. Siddique, H. Adeli. *Computational Intelligence: Synergies of Fuzzy Logic, Neural Networks and Evolutionary Computing*. Hoboken, NJ: Wiley, 2013.
- Squyres, S. W., Arvidson, R. E., Bollen, D., Bell III J. F., Brückner, J., Cabrol, N. A., et al. (2006). Overview of the Opportunity Mars Exploration Rover Mission to Meridiani Planum: Eagle crater to Purgatory ripple. *J. Geophys. Res.*, 111, E12S12. doi:10.1029/2006JE002771
- Hynek, B. M., Arvidson, R. E., & Phillips, R. J. (2002). Geologic setting and origin of Terra Meridiani hematite

- deposit on Mars. *J. Geophys. Res.*, 107(E10), 5088.
doi:10.1029/2002JE001891
- Maki, J. N., Bell III, J. F., Herkenhoff, K. E., Squyres, S. W., Kiely, A., Klimesh, M., et al. (2003). Mars Exploration Rover Engineering Cameras. *J. Geophys. Res.*, 108(E12), 8071. <http://dx.doi.org/10.1029/2003JE002077>.
- McEwen, A. (2007). Mars Reconnaissance Orbiter High Resolution Imaging Science Experiment, Experiment Data Record, MRO-M-HIRISE-2-EDR-V1.0, NASA Planetary Data System.
- Fenton, L. K., Michaels, T. I., & Chojnacki, M. (2015). Late Amazonian aeolian features, gradation, wind regimes, and Sediment State in the Vicinity of the Mars Exploration Rover Opportunity, Meridiani Planum, Mars. *Aeolian Research*, 16, 75–99. <https://doi.org/10.1016/j.aeolia.2014.11.004>

